ACS APPLIED MATERIALS & INTERFACES

Research Article

www.acsami.org

Solution-Processed LiF-Doped ZnO Films for High Performance Low Temperature Field Effect Transistors and Inverted Solar Cells

Jingjing Chang,[†] Zhenhua Lin,[‡] Chunxiang Zhu,[‡] Chunyan Chi,[†] Jie Zhang,[*,§] and Jishan Wu[*,†,§]

[†]Department of Chemistry, National University of Singapore, 3 Science Drive 3, 117543, Singapore

[‡]Department of Electrical and Computer Engineering, National University of Singapore, 10 Kent Ridge Crescent, Singapore 119260, Singapore

[§]Institute of Materials Research and Engineering, A*STAR, 3 Research Link, Singapore 117602, Singapore

Supporting Information

ABSTRACT: This paper reports that high performance metal oxide thin film transistors (TFTs) can be achieved by using LiF-doped ZnO thin films processed from aqueous solution. It was found that LiF doping at an appropriate amount enhanced the oxide film carrier concentration. The TFTs based on the 10 mol % LiF-doped ZnO thin films annealed at 300 °C revealed a good device performance with an average electron mobility of 8.9 cm^2 V^{-1} s^{-1} and a high on/off current ratio of 4 × 10^7, superior to the devices based on the nondoped ZnO TFTs (1.6 cm^2 V^{-1} s^{-1}). Even when annealed at 150 °C, the device still showed good transistor operation with an electron mobility of 0.54 cm^2 V^{-1} s^{-1}. The inverted bulk heterojunction solar cells based on P3HT:PCBM blend system fabricated using 10 mol % LiF doped ZnO as electron selective layer showed higher power conversion efficiency (η = 3.3%) than that from undoped ZnO thin films (η = 2.94%) due to enhanced short circuit current (J_{sc} = 10.55 mA/cm^2). Our results suggest that LiF incorporation can be a useful technique to produce high performance and low temperature solution-processed oxide TFTs and interface layer for solar cells.

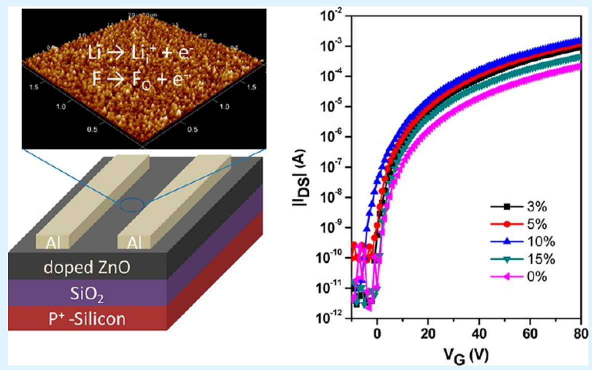

KEYWORDS: *ZnO, LiF, low temperature, field effect transistors, inverted solar cells*

INTRODUCTION

ZnO-based metal oxide semiconductors have been intensively studied as an active channel material for thin film transistor (TFTs) and solar cells.[1−3] Compared to n-type organic materials, inorganic ZnO shows several advantages such as being inexpensive, oxidation stable, and transparent in the visible region.[4] It can also combine with stable p-type semiconductor field effect transistors (FETs) for hybrid complementary inverters and logic circuits.[5] However, most ZnO films are deposited by expensive vacuum based techniques such as radio frequency (RF) sputtering,[6] pulsed laser deposition,[7] and physical vapor deposition,[8] or from a sol−gel precursor solution,[9] which usually needs high temperature annealing process to remove the carbon impurities and convert to ZnO. All these processes are incompatible with large area deposition and plastic substrates due to high cost and/or high temperature process. Therefore, solution-processed deposition technique is desirable, which is simple, controllable, and compatible with large area process. Previously, Keszler et al. reported a carbon free method with low temperature process.[10] However, the intrinsic mobility of ZnO is low which restricts its applications. Therefore, developing high performance ZnO thin films is essential in future plastics electronics.

Meanwhile, n-type metal oxides such as ZnO[11−13] and titanium oxide (TiO$_x$)[14,15] have been widely used for the electron selective buffer layer. In order to achieve efficient solar cell operation, the electron selective layer should work as a high conductive path for efficient electron extraction and has good hole blocking capability. Doped ZnO is a good choice compared to undoped ZnO due to higher charge carrier mobility and better film quality with less defect sites.

LiF as an inorganic salt has been frequently used as the electron selective layer in conventional solar cells.[16,17] The role of the LiF has been suggested to be that of controlling the work function of the cathode, causing chemical doping of the organic layer, protecting the polymer active layer from metal deposition, and introducing dipoles at the interface. Meanwhile, the two elements Li and F have been proved to be good doping candidates for ZnO thin film as n-type semiconductor materials. Recently, Li doped ZnO has been reported as a good n-type cationic doping source as electron donor with superior performance up to 50 cm^2 V^{-1} s^{-1}.[18,19] In addition, the fluorine (F), the radius of which is close to that of oxygen, has

Received: April 20, 2013
Accepted: June 17, 2013
Published: June 17, 2013

   dx.doi.org/10.1021/am4014488 | ACS Appl. Mater. Interfaces 2013, 5, 6687−6693

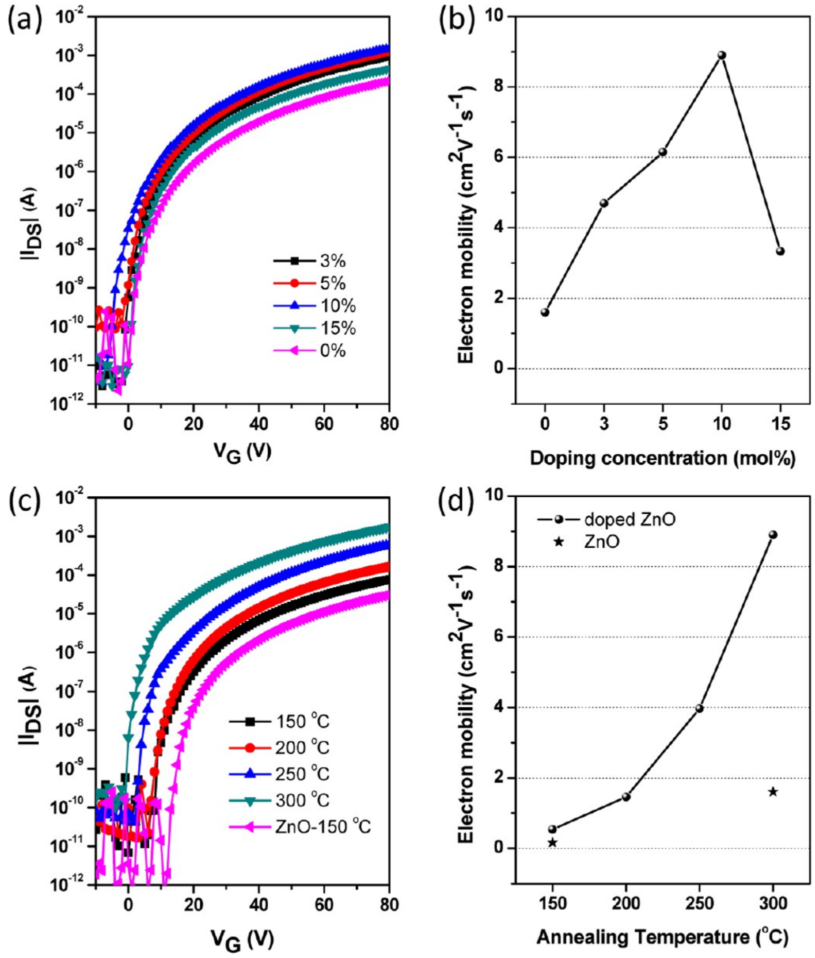

Figure 1. (a) Transfer characteristics of LiF doped ZnO TFTs with different doping concentrations. (b) Electron mobility of the LiF doped ZnO TFTs as a function of doping concentrations. (c) Transfer characteristics of 10 mol % LiF doped ZnO TFTs with different annealing temperatures. (d) Electron mobility of the 10 mol % doped ZnO TFTs as a function of annealing temperatures.

been proved to be an appropriate anionic doping candidate with lower lattice distortion compared with Sn, Ga, and In doping. Recent investigations revealed that incorporation of low concentration F in ZnO thin film could significantly improve the transmittance in visible region and the mobility of charge carries.[20,21]

In this study, we investigate the incorporation of LiF into ZnO using aqueous solution processing. The doped ZnO thin films exhibited electron mobility of 0.54 $cm^2\ V^{-1}\ s^{-1}$ when processed at 150 °C, and improved the short circuit current density (J_{sc}) of the inverted solar cell to 10.55 mA/cm^2 from 9.70 mA/cm^2. When the temperature of calcination increased to 300 °C, the average electron mobility could reach up to 8.9 $cm^2\ V^{-1}\ s^{-1}$, with a maximum value of 11.2 $cm^2\ V^{-1}\ s^{-1}$. The doping process is facile, and controllable, and the solution is easily prepared using commercial available materials.

■ EXPERIMENTAL SECTION

The precursor is prepared by dissolving the ZnO powder (Sigma Aldrich) in ammonium solution (Sigma Aldrich) to form 0.1 M ($Zn(NH_3)_4^{2+}$) complex. Then, different molar ratio of LiF or LiOH +NH_4F (Sigma Aldrich) was added to the precursor solution and refrigerated for several hours to promote the powder dissolution. For the device fabrication, a heavily doped p-type Si wafer (purchased from Silicon Quest International, Inc.) was served as the gate electrode and 200 nm of thermally grown SiO_2 was used as the dielectric layer. Prior to spin coating ZnO precursors, the Si/SiO_2 substrates were cleaned with acetone and isopropyl alcohol (IPA) and then treated with Ar plasma to facilitate the thin film formation. After that, ZnO precursors were spin-coated at 3000 rpm for 30 s to result in ZnO precursor thin film with around ~10 nm thickness. Then the substrates were annealed at 150−300 °C for 1 h. Finally, Al electrodes were deposited on the ZnO thin film with a shadow mask. The transistors were characterized with Keithley 4200 semiconductor analyzer in the N_2-filled glovebox. The field-effect mobility of the fabricated transistor was extracted using the following equation in the saturation regime from the gate sweep: $I_D = W/(2L)C_i\mu(V_G - V_T)^2$, where I_D is the drain current in the saturated regime, μ is the field-effect mobility, C_i is the capacitance per unit area of the gate dielectric layer (SiO_2, 200 nm, C_i = 17 nF cm^{-2}), V_G and V_T are gate voltage and threshold voltage, and W and L are channel width and length (500 μm/100 or 1000 μm/100 μm), respectively.

For inverted solar cell fabrication, ITO-coated glass substrates were cleaned by a routine solvent ultrasonic cleaning, sequentially with detergent, deionized water, acetone, and IPA in an ultrasonic bath for 15 min each. For solar cell fabrication, ZnO precursor was spin-coated at 3000 rpm for 30 s and annealed at 150 °C for 10 min. Following that, an active layer was deposited on top of the ZnO layer by spin-coating a solution of the P3HT (Rieke Metals) and PCBM (Nano-C) blend with a weight ratio of 1:1 in 1,2-dicholorobenzene (40 mg/mL) at 500 rpm for 130 s. The active layers were preannealed at 140 °C for 10 min. Finally, a MoO_3 layer (6 nm) and a Ag layer (100 nm) were deposited by using vacuum thermal evaporation. Device area was defined to be 9 mm^2 by a metal shadow mask. The current density−voltage (J−V) characteristics of the devices were measured using a Keithley 2400 parameter analyzer in the dark and under a simulated light (AM 1.5G) (SAN-EI ELECTRIC) with intensity of 100 mW/cm^2.

Surface properties of the ZnO film were characterized by two-dimensional X-ray diffraction (2D XRD) on the Bruker-AXS D8 DISCOVER GADDS instrument. The transmittance spectra of the ZnO films deposited onto quartz substrates were characterized by using a UV-3600 Shimadzu UV−vis-NIR spectrophotometer. The surface morphology and the roughness of the ZnO film deposited on silicon substrate were studied by tapping-mode atomic force microscopy (TM-AFM) performed on a Bruker ICON-PKG atomic force microscope. X-ray photoelectron spectroscopy (XPS) experiments were carried out at the Escalab 220i, with monochromatic Al Kα (1486.6 eV) as the radiation source. UPS experiments were carried out at the Escalab 220i, with He I (21.2 eV) as the excitation sources. Time-of-flight secondary ion mass spectrometry (TOF-SIMS) analysis was performed using a TOF-SIMS IV (ION-TOF) apparatus. TOF-SIMS was performed with the following conditions: bismuth gun, 25 keV, raster at 300 × 300 μm^2 for 300 scans, at positive polarity (good ion yield for Li ions, but poor ion yield for F).

■ RESULTS AND DISCUSSION

The electrical properties of the LiF doped ZnO films were characterized by bottom-gate top-contact thin film transistors.

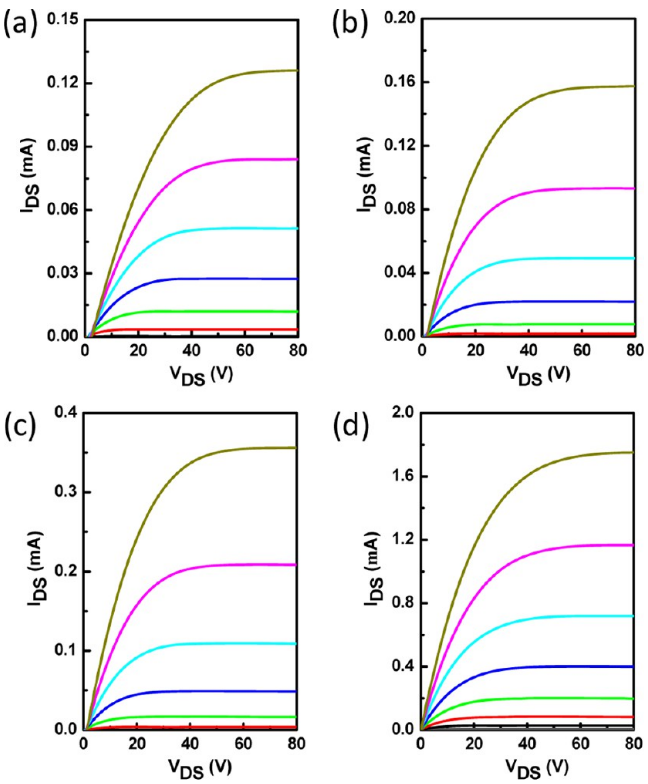

Figure 2. Output characteristics of the TFTs based on the 10 mol % LiF doped ZnO thin films under annealing temperature of 150 °C (a), 200 °C (b), 250 °C (c), and 300 °C (d) in air.

Figures 1 and 2 show the transfer and output characteristics for the as-fabricated devices with and without LiF doping (L = 100 um, W = 500 um). The TFTs exhibited excellent operating characteristics within the operating voltage. Linear behavior at low V_{DS} indicates an ohmic contact at the Al/ZnO interface. The dopant concentration has significant effect on the device performance (Figure 1a,b and Figure S1 in the Supporting Information). The drain current increased upon introducing the LiF into ZnO up to 10 mol %. However, when the doping concentration increased to 15 mol %, the current decreased significantly due to more charge traps formed by excess LiF impurities. In this case, the Li (F) appears to exist at substitutional (interstitial) sites as an acceptor.[20−22] After optimization, the 10 mol % LiF doped ZnO films after annealing at 300 °C exhibited the best performance with average mobility of 8.9 $cm^2\ V^{-1}\ s^{-1}$ with a threshold voltage (V_{th}) of 20 V, and current on/off ratio of 10^7−10^8. The maximum electron mobility could reach up to 11.2 $cm^2\ V^{-1}\ s^{-1}$. This value is among the highest values reported for the low temperature solution-processed ZnO based TFT devices.[23] The operational stability of these thin films was also checked with on/off cycle test in the ambient conditions. As shown in Figure 3, the current of the 10 mol % LiF doped ZnO thin film TFT only exhibited slightly current decrease in the initial stage of the on/off cycles, which understood as a "burn-in" effect at the initial stage for all materials and interfaces to be stabilized under the constant voltage bias.

For the doping mechanism, it has been proved that the Li in the ZnO matrix prefers interstitial sites to substitutional sites due to low electron affinity. When Li occupies the interstitial sites ($Li \rightarrow Li_i^+ + e^-$), it can produce electrons and improve the carrier concentration, which results in high electron mobility.[22] Meantime, the results showed that F occupied in substitutional oxygen sites ($F \rightarrow F_O + e^-$) is more energetically favorable compared to fluorine interstitial sites (F_i).[20] The F_O can effectively diminish oxygen vacancies and decrease the absorption in visible region. The enhancement of the carrier concentration could be explained by the surface passivation effect and the removal of the in-grain scattering centers. Therefore, the codoping of cation (Li) and anion (F) could have synergistic effect to combine both advantages, which not only increases the carrier concentration, but also decreases the optical absorption. This is desirable for the transparent TFTs and inverted solar cells.

In order to investigate the low temperature processability, the TFT devices with different annealing temperature ranging from 150 to 300 °C were fabricated and the results were shown in Figure 1c,d and Figure S2 in the Supporting Information. Electron mobility up to 0.54 $cm^2\ V^{-1}\ s^{-1}$ could be achieved with good transistor operation even when annealed at 150 °C, indicating that low temperature solution-processed oxide TFTs on flexible substrates could be achievable with carbon-free ZnO thin films as the active layer. When the annealing temperature increased, the electron mobility of the ZnO films increased significantly from 0.54 to 8.9 $cm^2\ V^{-1}\ s^{-1}$ when the thin films were annealed at 300 °C. This could be ascribed to the increased crystallinity and particle size. Consistent with these results, the threshold voltage and turn-on voltage (V_{on}) gradually decrease with the annealing temperature increase. The charge density in the channel layer, corresponding to the turn-on voltage, increased to $7.44 \times 10^{17}\ cm^{-3}$ when the doping ratio increased to 10% using the equation $N_T = C_i V_{on}/(qt)$, where C_i is the gate insulator capacitance per unit area, q is the elementary charge, and t is the thickness of active layer. The increment of carrier concentration, which was induced by interstitial Li doing and substitutional F doping, could enhance the field effect mobility.[24]

The morphology and microstructure of the thin films surface with different annealing temperatures and different doping concentrations were investigated by the tapping-mode AFM and 2D XRD. For different doping concentrations, the topography images almost do not show changes and reveal good quality films with a root-mean-square (rms) of surface

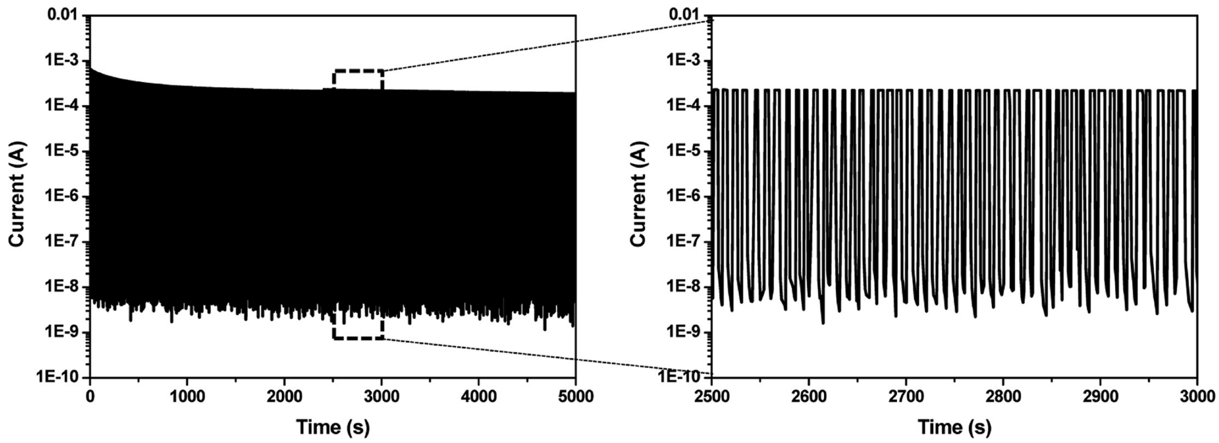

Figure 3. Dynamic stress test of a 10 mol % LiF doped ZnO TFT during continuous cycling between ON (V_G = 60 V) and OFF states (V_G = 0 V).

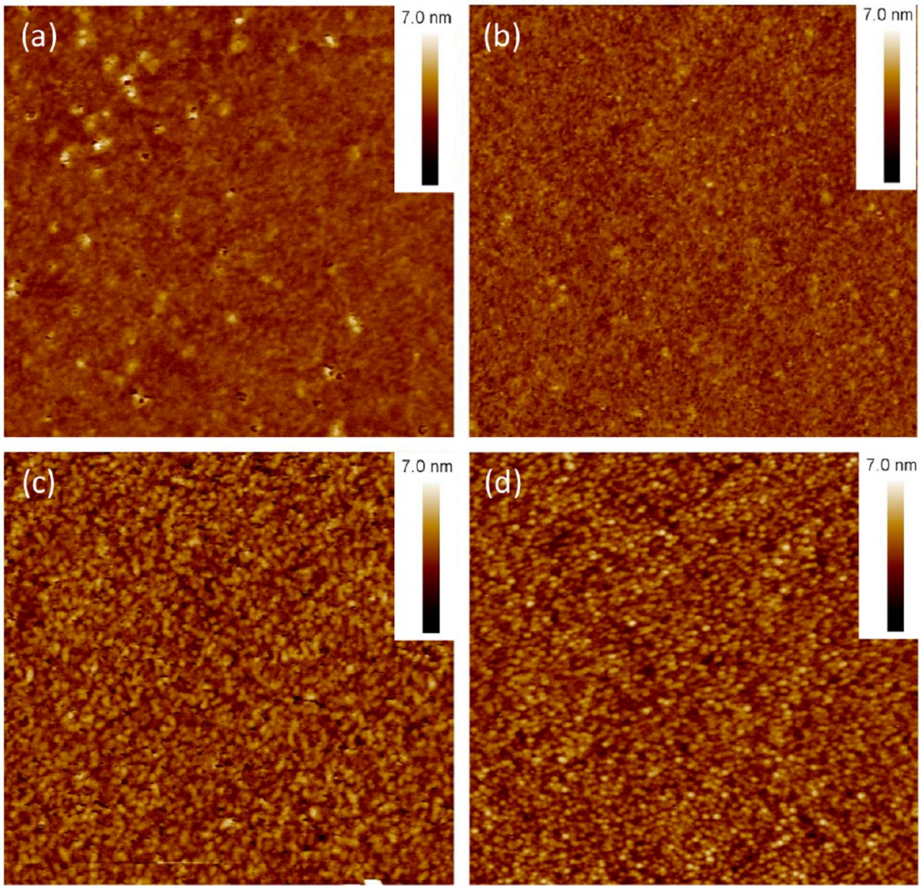

Figure 4. AFM images (2 μm × 2 μm) of LiF doped ZnO thin films annealed at 150 °C (a), 200 °C (b), 250 °C (c), and 300 °C (d).

roughness of 0.47−0.51 nm (Figure 4 and Figure S3−S4 in the Supporting Information). However, the surface morphologies are more related to the annealing temperature. Low temperature (150 °C) annealing gave a smoother and featureless morphology. When the temperature was increased to 250 °C, the film became more crystalline and had a distinct granular structure (Figure 4). The surface roughness and grain size increased with the increasing of the annealing temperatures. The rms values of surface roughness at different annealing temperatures were 0.267 nm (150 °C), 0.313 nm (200 °C), 0.403 nm (250 °C), and 0.485 nm (300 °C), and the grain sizes were estimated to be about 22−36 nm at 300 °C. The microstructures of the thin films were evaluated by 2D XRD, the nanoparticle powder of pristine and doped ZnO showed crystalline wurzite structure with weak (002) orientation. However, the thin film annealing at 300 °C exhibited substantial *c*-axis oriented growth with preferential (002) orientation (Figure S5−6 in the Supporting Information). The result is consistent with literature reported.[21] The chemical structures of LiF doped ZnO were further studied using XPS analysis; as shown in Figure S7 (Supporting Information), due to resolution problem, the F 1s and Li 1s peaks were not obviously detected. To confirm the doping ions exist in ZnO films, TOF-SIMS measurements were carried out, and the

dx.doi.org/10.1021/am4014488 | ACS Appl. Mater. Interfaces 2013, 5, 6687−6693

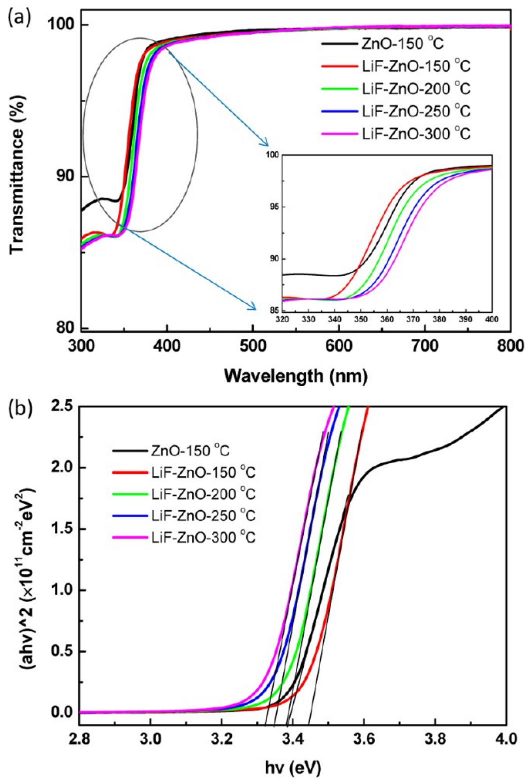

Figure 5. (a) Optical transmission spectra of the ZnO and 10 mol % LiF-doped ZnO thin films on quartz substrates after annealing at different temperatures. (b) Absorption coefficient as a function of photon energy.

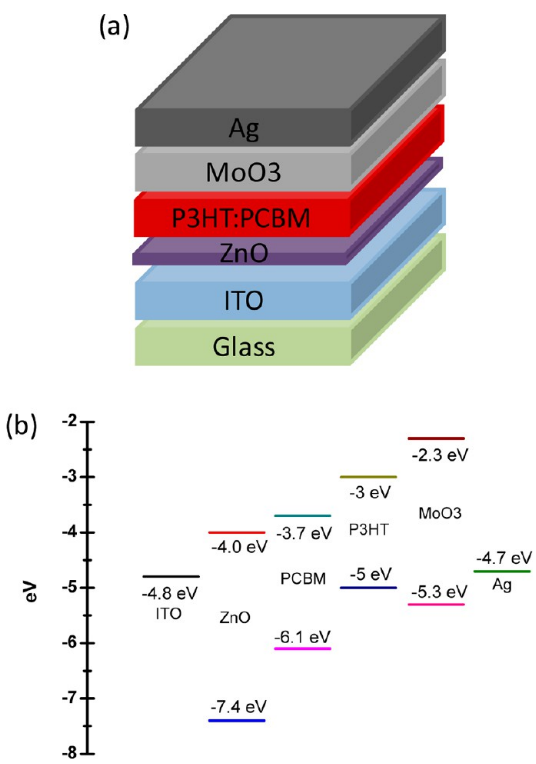

Figure 6. (a) Device structure of the inverted P3HT:PCBM solar cell and (b) energy level diagram of the component materials used in device fabrication.

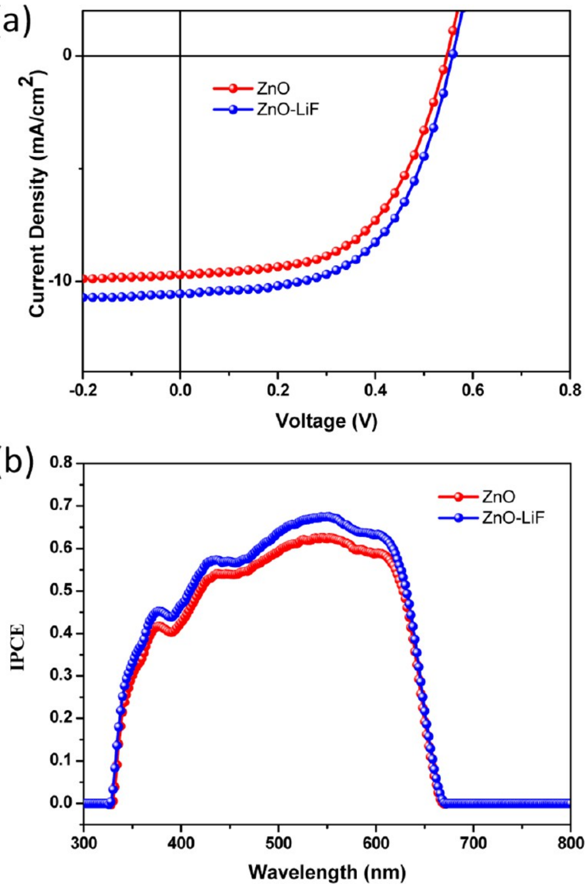

Figure 7. (a) *J*−*V* characterisctics of inverted P3HT:PCBM solar cells incorporating undoped/doped ZnO films. (b) IPCE spectra of inverted P3HT:PCBM solar cells.

results are shown in Figure S8−S9 in the Supporting Information. The Li ion could be well observed, and the depth profile also gave good evidence that high intensity of Li cations was detected.

The optical transmittance was measured to investigate the doping effect of LiF on the ZnO optical band gap. Figure 5a shows the transmittance spectra of the ZnO film with/without LiF doping on the quartz substrates after annealing at the selected temperature (150 −300 °C) for 10 min. It can be seen that all ZnO films have good transmittances above 95% over the visible wavelength range. From the transmittance spectra, the absorption coefficient as a function of photon energy has been plotted (Figure 5b), from which the optical band gap of each ZnO film can be easily measured. The absorption coefficient α can be calculated as follows:[25] $T = A\ \exp(-\alpha d)$, where T is the transmittance of the ZnO film, A is a constant and approximately unity, and d is the film thickness. The optical band gap of the ZnO films is determined by applying the Tauc model[26] and the Davis Mott model[27] in the high absorbance region: $\alpha h\nu = D(h\nu - E_g)_n$, where $h\nu$ is the photon energy, E_g is the optical band gap, D is a constant, and n equals to 1/2. The direct optical band gap of the ZnO thin films with/without LiF doping was obtained by plotting $(\alpha h\nu)^2$ versus $h\nu$, as shown in Figure 5b. The E_g value can be obtained by extrapolating the linear portion to the photon energy axis. It can be seen that the band gaps of the ZnO films slightly increased to 3.441 eV from 3.386 eV after doping with LiF. With annealing temperature increase, the optical band gap values of the doped ZnO films

Table 1. Device Photovoltaic Performance Parameters of Inverted P3HT:$PC_{60}BM$ Solar Cells Incorporating Undoped/Doped ZnO Films as the Electron Transport Layer

	band gap (eV)	μ ($cm^2 V^{-1} s^{-1}$)	J_{sc} (mA/cm^2)	V_{oc} (V)	FF	η (%)
ZnO	3.386	0.18	9.70	0.54	0.56	2.94
ZnO-LiF	3.441	0.54	10.55	0.56	0.56	3.31

were 3.376 eV (200 °C), 3.343 eV (250 °C), and 3.325 eV (300 °C). The widening of the optical band gap after doping could be explained by Burstein–Moss effects.[28] The doubly occupied state is restricted which needs extra energy to excite valence electrons to higher states in the conduction band.

The high performance LiF doped ZnO thin film showed great potential as electron selective layer in inverted solar cells. The devices were fabricated using P3HT:PCBM system. Figure 6a and b illustrates the schematic device structure and the band diagram of the inverted OSCs, respectively. The valence band maximum (VBM) was estimated from UPS (Figure S10 in the Supporting Information), and the band gap (E_g) was obtained from the UV absorption edge. The VBM and the conduction band minimum (CBM) of the ZnO film are 7.4 ± 0.02 and 4.0 ± 0.02 eV, respectively. The current density–voltage (J–V) characteristics of the devices incorporating 10 mol % LiF doped ZnO buffer layers are shown in Figure 7a and Figure S11 in the Supporting Information, and extracted device parameters are summarized in Table 1. Compared to the devices using ZnO as the electron selective layer, the doped ZnO gave a much higher J_{sc} (10.55 mA/cm^2) than the reference devices due to the increased charge carrier mobility. V_{oc} shows only slight increase, which finally resulted in a power conversion efficiency of 3.3%. Incident photon-to-current conversion efficiency (IPCE) spectra are shown in Figure 7b. The devices comprising LiF doped ZnO buffer layer showed the maximum IPCE of 68% at the wavelength of 550 nm, indicating an efficient photon-to-current conversion. The integrated IPCE values are all in good agreement with the measured J_{sc}.

CONCLUSION

In summary, LiF-doped ZnO thin films have been successfully prepared from aqueous solution at low processing temperature. LiF doping at the appropriate amounts enhanced the oxide film quality and reduced defect sites. The TFTs based on LiF doped ZnO thin films revealed largely improved device performance with average electron mobility up to 8.9 $cm^2 V^{-1} s^{-1}$ compared with the mobility of 1.6 $cm^2 V^{-1} s^{-1}$ for nondoped ZnO TFTs. The inverted solar cell fabricated using LiF doped ZnO as electron selective layer showed enhanced performance (η = 3.3%) compared to the undoped ZnO thin film (η = 2.94%). Our results suggest that LiF doping can be a useful technique to produce more reliable and low temperature solution-processed oxide semiconductor TFTs and solar cells.

ASSOCIATED CONTENT

Supporting Information

TFT device characteristics, AFM images, 2D XRD patterns, XPS spectra, TOF-SIMS results, UPS spectrum, and solar cell I-V characteristics. This material is available free of charge via the Internet at http://pubs.acs.org.

AUTHOR INFORMATION

Corresponding Author

*Fax: +65 6779 1691. Tel: +65 6516 2677. E-mail: chmwuj@nus.edu.sg, wuj@imre.a-star.edu.sg (J.W.); zhangj@imre.a-star.edu.sg (J.Z.).

Notes

The authors declare no competing financial interest.

ACKNOWLEDGMENTS

This work was financially supported by MOE Tier 2 grant (MOE2011-T2-2-130), IMRE Core Funding (IMRE/12-1P0902), and A*STAR SERC TSRP grant (Grant #102 170 0137).

REFERENCES

(1) Kim, M. G.; Kanatzidis, M. G.; Facchetti, A.; Marks, T. J. *Nat. Mater.* **2011**, *10*, 382–387.
(2) Banger, K.; Yamashita, Y.; Mori, K.; Peterson, R.; Leedham, T.; Rickard, J.; Sirringhaus, H. *Nat. Mater.* **2011**, *10*, 45–50.
(3) Huang, J.; Yin, Z.; Zheng, Q. *Energy Environ. Sci.* **2011**, *4*, 3861–3877.
(4) Fortunato, E.; Barquinha, P.; Martins, R. *Adv. Mater.* **2012**, *24*, 2945–2986.
(5) Smith, J.; Bashir, A.; Adamopoulos, G.; Anthony, J. E.; Bradley, D. D. C.; Hamilton, R.; Heeney, M.; McCulloch, I.; Anthopoulos, T. D. *Adv. Mater.* **2010**, *22*, 3598–3602.
(6) Carcia, P. F.; McLean, R. S.; Reilly, M. H.; Nunes, G. *Appl. Phys. Lett.* **2003**, *82*, 1117.
(7) Nishii, J.; Hossain, F. M.; Takagi, A.; Aita, T.; Saikusa, K.; Ohmaki, Y.; Ohkubo, I.; Kishimoto, S.; Ohtomo, A.; Fukumura, T.; Matsukura, F.; Ohno, Y.; Koinuma, H.; Ohno, H.; Kawasaki, M. *Jpn. J. Appl. Phys.* **2003**, *42*, 347–349.
(8) Jo, J.; Seo, O.; Choi, H.; Lee, B. *Appl. Phys. Express* **2008**, *1*, 041202.
(9) Ong, B. S.; Li, C. S.; Li, Y. N.; Wu, Y. L.; Loutfy, R. J. *J. Am. Chem. Soc.* **2007**, *129*, 2750–2751.
(10) Meyers, S. T.; Anderson, J. T.; Hung, C. M.; Thompson, J.; Wager, J. F.; Keszler, D. A. *J. Am. Chem. Soc.* **2008**, *130*, 17603–17609.
(11) Liang, Z.; Zhang, Q.; Wiranwetchayan, O.; Xi, J.; Yang, Z.; Park, K.; Li, C.; Cao, G. *Adv. Funct. Mater.* **2012**, *22*, 2194–2201.
(12) Sun, Y.; Seo, J. H.; Takacs, C. J.; Seifter, J.; Heeger, A. J. *Adv. Mater.* **2011**, *23*, 1679–1683.
(13) Shao, S.; Zheng, K.; Pullerits, T.; Zhang, F. *ACS Appl. Mater. Interfaces* **2013**, *5*, 380–385.
(14) Sun, H.; Weickert, J.; Hesse, H. C.; Schmidt-Mende, L. *Sol. Energy Mater. Sol. Cells* **2011**, *95*, 3450–3454.
(15) Liu, J.; Shao, S.; Meng, B.; Fang, G.; Xie, Z.; Wang, L.; Li, X. *Appl. Phys. Lett.* **2012**, *100*, 213906.
(16) Brabec, C. J.; Shaheen, S. E.; Winder, C.; Sariciftci, N. S.; Denk, P. *Appl. Phys. Lett.* **2002**, *80*, 1288–1290.
(17) Ahlswede, E.; Hanisch, J.; Powalla, M. *Appl. Phys. Lett.* **2007**, *90*, 163504.
(18) Adamopoulos, G.; Thomas, S.; Wobkenberg, P. H.; Bradley, D. D. C.; McLachlan, M. A.; Anthopoulos, T. D. *Adv. Mater.* **2011**, *23*, 1894–1898.
(19) Adamopoulos, G.; Bashir, A.; Thomas, S.; Gillin, W. P.; Georgakopoulos, S.; Shkunov, M.; Baklar, M. A.; Stingelin, N.; Maher, R. C.; Cohen, L. F.; Bradley, D. D. C.; Anthopoulos, T. D. *Adv. Mater.* **2010**, *22*, 4764–4769.

(20) Liu, B.; Gu, M.; Liu, X.; Huang, S.; Ni, C. *Appl. Phys. Lett.* **2010**, *97*, 122101.
(21) Ilican, S.; Caglar, Y.; Caglar, M.; Yakuphanoglu, F. *Appl. Surf. Sci.* **2008**, *255*, 2353−2359.
(22) Park, S. Y.; Kim, K.; Lim, K.; Kim, B. J.; Lee, E.; Cho, J. H.; Kim, Y. S. *J. Mater. Chem. C* **2013**, *1*, 1383−1391.
(23) Park, S.; Kim, B. J.; Kim, K.; Kang, M. S.; Lim, K.; Lee, T.; Myoung, J. M.; Baik, H. K.; Cho, J. H.; Kim, Y. S. *Adv. Mater.* **2012**, *24*, 834−838.
(24) Alder, D.; Flora, L. P.; Senturia, S. D. *Solid State Commun.* **1973**, *12*, 9−12.
(25) Tan, S. T.; Chen, B. J.; Sun, X. W.; Fan, W. J. *J. Appl. Phys.* **2005**, *98*, 013505.
(26) Tauc, J. *Amorphous and Liquid Semiconductors*; Plenum: London, 1974.
(27) David, E. A.; Mott, N. F. *Philos. Mag.* **1970**, *22*, 903−922.
(28) Sernelius, B. E.; Berggren, K. F.; Jin, Z. C.; Hamberg, I.; Granqvist, C. G. *Phys. Rev. B: Condens. Matter Mater. Phys.* **1988**, *37*, 10244−10248.